PCCP

Mixed annihilation electrogenerated chemiluminescence of iridium(III) complexes

Journal:	*Physical Chemistry Chemical Physics*
Manuscript ID	CP-ART-03-2018-001737.R1
Article Type:	Paper
Date Submitted by the Author:	24-Jun-2018

Complete List of Authors:	Soulsby, Lachlan; Deakin University, School of Life and Environmental Sciences; Hayne, David; Deakin University, School of Life and Environmental Sciences Doeven, Egan; Deakin University, Centre for Chemistry and Biotechnology Wilson, David; La Trobe University, Chemistry Agugiaro, Johnny; La Trobe University Connell, Timothy ; RMIT Univeristy , Chemistry ; CSIRO, Manufacturing Chen, Lifen; Deakin University, School of Life and Environmental Sciences Hogan, Conor; La Trobe University, Department of Chemistry and Physics Kerr, Emily; Monash University, Monash Institute of Pharmaceutical Sciences Adcock, Jacqui; Deakin University, School of Life and Environmental Sciences Donnelly, Paul; University of Melbourne, School of Chemistry White, Jonathan; University of Melbourne, School of Chemistry Francis, Paul; Deakin University, School of Life and Environmental Sciences

PCCP

PAPER

Mixed annihilation electrogenerated chemiluminescence of iridium(III) complexes

Received 00th January 20xx,
Accepted 00th January 20xx

DOI: 10.1039/x0xx00000x

www.rsc.org/

Lachlan C. Soulsby,[a] David J. Hayne,[a] Egan H. Doeven,[b] David J.D. Wilson,[c] Johnny Agugiaro,[c] Timothy U. Connell,[d,†] Lifen Chen,[a] Conor F. Hogan,[c] Emily Kerr,[a,‡] Jacqui L. Adcock,[a] Paul S. Donnelly,[e] Jonathan M. White[e] and Paul S. Francis*[a]

Previously reported annihilation ECL of mixtures of metal complexes have generally comprised $Ir(ppy)_3$ or a close analogue as a higher energy donor/emitter (green/blue light) and $[Ru(bpy)_3]^{2+}$ or its derivative as a lower energy acceptor/emitter (red light). In contrast, here we examine $Ir(ppy)_3$ as the lower energy acceptor/emitter, by combining it with a second Ir(III) complex: $[Ir(df\text{-}ppy)_2(ptb)]^+$ (where ptb = 1-benzyl-1,2,3-triazol-4-ylpyridine). The application of potentials sufficient to attain the first single-electron oxidation and reduction products can be exploited to detect $Ir(ppy)_3$ at orders of magnitude lower concentration, or enhance its maximum emission intensity at high concentration far beyond that achievable through conventional annihilation ECL of $Ir(ppy)_3$ involving comproportionation. Moreover, under certain conditions, the colour of the emission can be selected through the applied electrochemical potentials. We have also prepared a novel Ir(III) complex with a sufficiently low reduction potential that the reaction between its reduced form and $Ir(ppy)_3^+$ cannot populate the excited state of either luminophore. This enabled, for the first time, the exclusive formation of either excited state through the application of higher cathodic or anodic potentials, but in both cases, the ECL was greatly diminished by parasitic dark reactions.

Introduction

Iridium(III) complexes have emerged as promising alternatives to the traditional ruthenium(II) complexes utilised in electrogenerated chemiluminescence (ECL) systems.[1, 2] The introduction of these novel electrochemiluminophores was predominantly focussed on improving ECL efficiencies,[3, 4] but Bruce and Richter were also quick to show that the wider range of emission colours from Ir(III) complexes could be exploited for simultaneous multi-colour co-reactant ECL from mixtures of Ir(III) and Ru(II) complexes.[5] Despite the promising early demonstration by Richter's group and the plethora of new Ir(III) and other metal complexes that were synthesised and tested in subsequent ECL studies, surprisingly few multi-colour metal-complex ECL systems were reported over the following decade.[6]

In 2012, however, several co-reactant ECL systems were reported in which the distinct redox character of the electrochemiluminophores was exploited to control the formation of different emitting species,[7] stimulating new interest in the development of multi-colour ECL systems.[2, 8] Subsequent reports have included electrochemically tuneable multi-coloured co-reactant ECL from multiple metal complexes,[9] heterodinuclear Ru(II)/Ir(III) complexes,[10] a single Ir(III) complex,[11] and combinations of different ECL systems.[12] Moreover, the annihilation ECL of mixtures of Ru(II) and Ir(III) complexes was explored for the first time.[13-17]

Unlike co-reactant ECL, where only an oxidative or a reductive potential is applied, the annihilation mode of ECL involves the alternating application of oxidative and reductive potentials, with subsequent reactions between the oxidised and reduced metal complexes generating the excited state responsible for the emission.[1, 2, 8] In mixed annihilation ECL systems, the multiple oxidation and reduction potentials of the metal complexes offer a simple means to control the generation of more than one excited state, and therefore the overall colour of the emission. With this in mind, Moon *et al.*[13] sought to fabricate a colour-tuneable ECL-based light-emitting device comprising two luminophores ($[Ru(bpy)_3]Cl_2$ and $[Ir(df\text{-}ppy)_2(bpy)](PF_6)$; see Fig. 1a). Under the applied conditions, the orange-red ECL of the Ru(II) complex was enhanced two-fold, but the characteristic green ECL from the Ir(III) complex was

[a] Deakin University, Geelong, Victoria 3220, Australia. School of Life and Environmental Sciences, Faculty of Science, Engineering and Built Environment.
[b] Deakin University, Geelong, Victoria 3220, Australia. Centre for Regional and Rural Futures, Faculty of Science, Engineering and Built Environment.
[c] Department of Chemistry and Physics, La Trobe Institute for Molecular Science, La Trobe University, Melbourne, Victoria 3086, Australia.
[d] Manufacturing Business Unit, Commonwealth Scientific and Industrial Research Organisation (CSIRO), Clayton, Victoria 3168, Australia.
[e] School of Chemistry and Bio21 Molecular Science and Biotechnology Institute, The University of Melbourne, Victoria 3010, Australia.
† Current affiliation: RMIT University, Melbourne, Victoria 3001 Australia.
‡ Current affiliation: Monash Institute of Pharmaceutical Sciences, Monash University, Parkville, Victoria 3052, Australia; and CSIRO, Clayton, Victoria 3168, Australia

Electronic Supplementary Information (ESI) available: [details of any supplementary information available should be included here]. See DOI: 10.1039/x0xx00000x

not observed. Similarly, Swanick *et al.*[15] examined the annihilation and co-reactant ECL of a [Ru(dtb-bpy)$_3$][Ir(ppy)$_2$(CN)$_2$]$_2$ 'soft salt' (and the related combination of [Ru(dtb-bpy)$_3$](PF$_6$) and TBA[Ir(ppy)$_2$(CN)$_2$] (Fig. 1b)) dissolved in acetonitrile and observed only the orange-red emission of the Ru(II) complex.

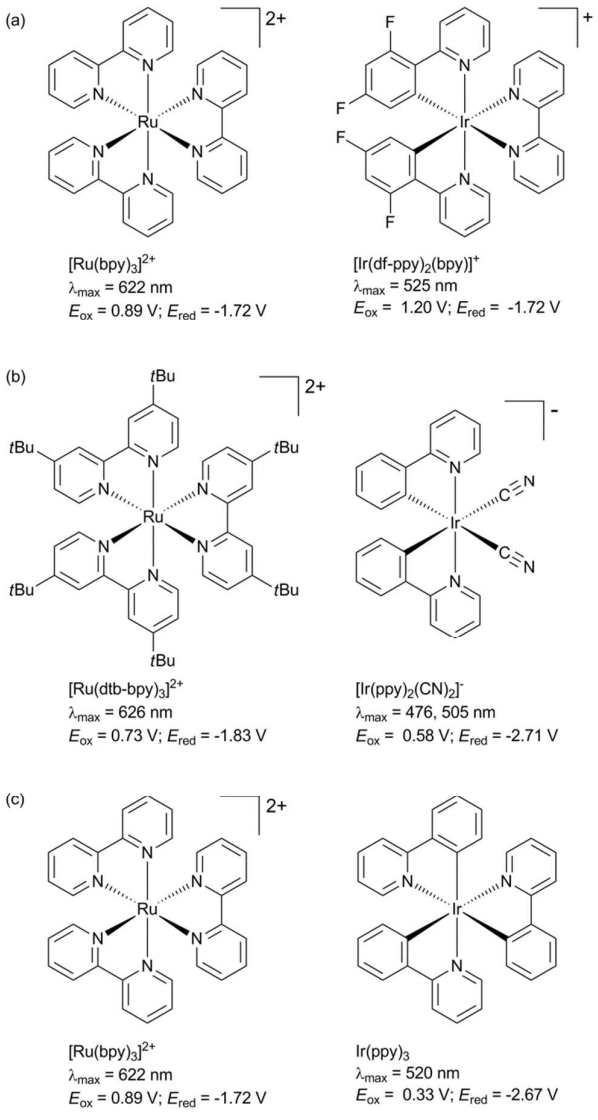

Figure 1. Combinations of metal complexes used in three previous annihilation ECL studies.[13-16] Electrochemical potentials are referenced to $Fc^{0/+}$. Data from reference [16].

We previously investigated the annihilation ECL of $[Ru(bpy)_3]^{2+}$ and various Ir(III) complexes (*e.g.*, Fig. 1c), and under suitable conditions, we observed emission from one or both luminophores, depending on which electrochemical potentials were applied.[14] In a mixture of $[Ru(bpy)_3]^{2+}$ and $Ir(ppy)_3$, for example, the Ir(III) complex is easier to oxidise and the Ru(II) complex is more readily reduced (Fig. 2b). We can therefore alternately apply positive and negative potentials that will only oxidise the Ir(III) complex and only reduce the Ru(II) complex. Subsequent electron transfer between these two species provides sufficient energy to attain the excited state $[Ru(bpy)_3]^{2+}$* (Equations 1-4), but not $Ir(ppy)_3$*. Thus, only the characteristic orange-red luminescence of the Ru(II) complex (Fig. 2a) was observed.[14]

$$[Ru(bpy)_3]^{2+} + e^- \rightarrow [Ru(bpy)_3]^{+} \quad (1)$$
$$Ir(ppy)_3 - e^- \rightarrow [Ir(ppy)_3]^{+} \quad (2)$$
$$[Ir(ppy)_3]^{+} + [Ru(bpy)_3]^{+} \rightarrow Ir(ppy)_3 + [Ru(bpy)_3]^{2+}* \quad (3)$$
$$[Ru(bpy)_3]^{2+}* \rightarrow [Ru(bpy)_3]^{2+} + h\nu \quad (4)$$

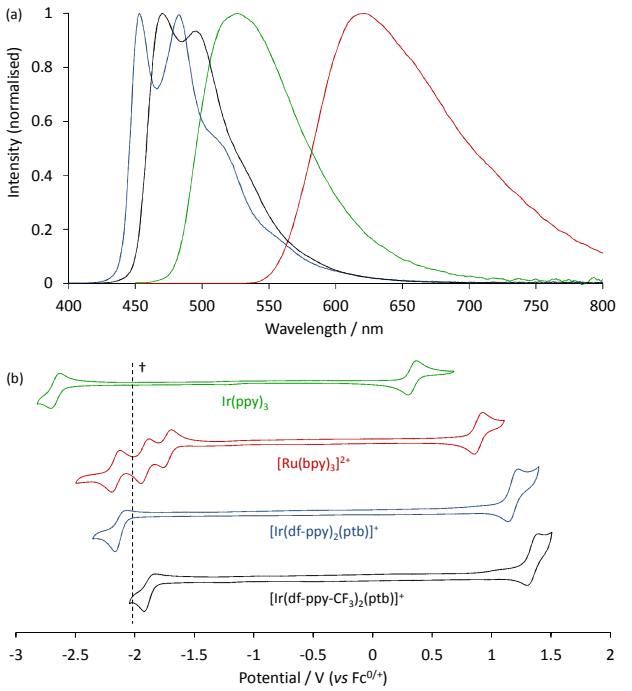

Figure 2. (a) Corrected photoluminescence emission spectra and (b) cyclic voltammograms for $[Ru(bpy)_3]^{2+}$ (red line), $Ir(ppy)_3$ (green line), $[Ir(df\text{-}ppy)_2(ptb)]^+$ (blue line) and $[Ir(df\text{-}ppy\text{-}CF_3)_2(ptb)]^+$ (black line) in dry acetonitrile at room temperature. The spectra were obtained using a metal complex concentration of 10 μM, using excitation wavelengths of 450, 350, 310 and 260 nm, respectively, with appropriate excitation and emission filters (see also Fig. S1). The CVs were obtained at 200 μM with 0.1 M $TBAPF_6$ supporting electrolyte, at a scan rate of 0.1 V s^{-1}, using a glassy carbon working electrode, platinum wire counter electrode and silver wire reference electrode. Prior to collecting the CVs, the solutions were degassed for 15 min. The dotted line (†) shows the minimum potential required to generate $Ir(ppy)_3$* upon reaction with $Ir(ppy)_3^+$. For example, the $[Ru(bpy)_3]^{+/0}$ couple is on right side of the line, and so the reaction of $[Ru(bpy)_3]^0$ and $Ir(ppy)_3^+$ does not generate $Ir(ppy)_3$*, whereas the $[Ru(bpy)_3]^{0/-}$ couple is on the left side of the line, and the reaction of $[Ru(bpy)_3]^-$ and $Ir(ppy)_3^+$ can generate $Ir(ppy)_3$* (*i.e.* Equation 7).

Simple estimations of the exergonicity[14, 16, 18] of reactions between the redox states available in this system (Fig. 2b) indicate that the least powerful reductant capable of generating $Ir(ppy)_3$* upon reaction with $[Ir(ppy)_3]^+$ was the $3e^-$ reduced state of $[Ru(bpy)_3]^{2+}$ (Equations 5-8). When the cathodic pulse was moved sufficiently negative to generate $[Ru(bpy)_3]^-$, the green emission from $Ir(ppy)_3$* (*via* Equation 7) and the orange-red emission from $[Ru(bpy)_3]^{2+}$* (*via* Equation 3) both occurred, which was perceived visually as yellow light.

$$[Ru(bpy)_3]^{+} + e^- \rightarrow [Ru(bpy)_3]^{0} \quad (5)$$
$$[Ru(bpy)_3]^{0} + e^- \rightarrow [Ru(bpy)_3]^{-} \quad (6)$$

$[Ir(ppy)_3]^+ + [Ru(bpy)_3]^- \rightarrow Ir(ppy)_3^* + [Ru(bpy)_3]^0$ (7)

$Ir(ppy)_3^* \rightarrow Ir(ppy)_3 + h\nu$ (8)

When the cathodic pulse was moved further negative to reduce $Ir(ppy)_3$ (Fig. 2b), the emission from the green luminophore was markedly increased through its comproportionation (Equation 9), and the formation of $[Ru(bpy)_3]^{2+*}$ was inhibited by an irreversible fourth reduction of the ruthenium complex, resulting in a predominantly green emission.[16]

$[Ir(ppy)_3]^+ + [Ir(ppy)_3]^- \rightarrow Ir(ppy)_3^* + Ir(ppy)_3$ (9)

The investigations of multi-colour annihilation ECL with mixtures of metal complexes to date[13-16] have each focussed on a combination of $[Ru(bpy)_3]^{2+}$ (or its di-*t*-butyl-bipyridine derivative) and an Ir(III) complex that emits green or blue light. In each case, electron and/or energy transfer between iridium and ruthenium species favoured the formation of the excited state of the Ru(II) complex,[16] often resulting in emission exclusively from that luminophore.[13, 15] Moreover, in each case, the reaction between the most readily formed oxidation and reduction products provided sufficient energy to generate the excited state ruthenium complex (*e.g.*, Equation 3). It was therefore not possible to apply potentials that would generate the excited state Ir(III) complex in the absence of any energetically feasible pathways to form the exited state Ru(II) complex.

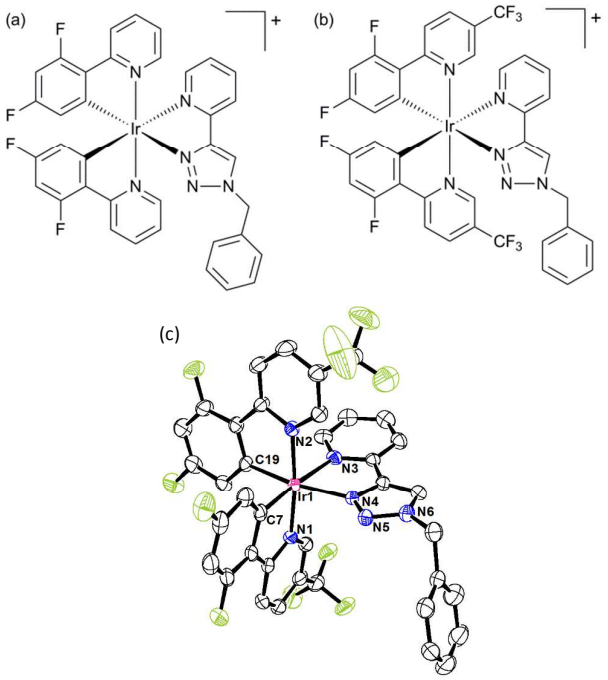

Figure 3. (a) $[Ir(df\text{-}ppy)_2(ptb)]^+$ and (b) $[Ir(df\text{-}ppy\text{-}CF_3)_2(ptb)]^+$, which were combined with $Ir(ppy)_3$ in this study of mixed annihilation ECL. (c) ORTEP representation of the cation $[Ir(df\text{-}ppy\text{-}CF_3)_2(ptb)]^+$ with thermal ellipsoids at the 40% probability level. Hydrogen atoms and solvent molecules omitted for clarity.

Herein we first demonstrate the annihilation ECL of a mixture of two Ir(III) complexes: $Ir(ppy)_3$ (Fig. 1c, right) and $[Ir(df\text{-}ppy)_2(ptb)]^+$ (Fig. 3a), which emit green and blue light, respectively. Unlike previous reports, in which the $Ir(ppy)_3$ complex was the higher energy emitter that was partially quenched in the presence of the Ru(II) complex, in this study, $Ir(ppy)_3^*$ is the longer wavelength emitter, which we anticipated to be favoured over the formation of the higher energy $[Ir(df\text{-}ppy)_2(ptb)]^{+*}$. Secondly, we prepared a novel blue luminophore ($[Ir(df\text{-}ppy\text{-}CF_3)_2(ptb)]^+$; Fig. 3b) with a reduction potential of sufficiently low magnitude that the reaction between its reduced form and the oxidised $Ir(ppy)_3^+$ cannot attain the excited state of either luminophore (*i.e.* neither $[Ir(df\text{-}ppy\text{-}CF_3)_2(ptb)]^{+*}$ nor $Ir(ppy)_3^*$). This enables the selective formation of either excited state through the application of higher cathodic or anodic potentials.

Results and discussion

Annihilation ECL from a mixture of two Ir(III) complexes

For these experiments, we selected $Ir(ppy)_3$ and $[Ir(df\text{-}ppy)_2(ptb)]^+$, as two complexes possessing sufficiently dissimilar emission wavelengths (Fig. 2a and S1; Table 1) and redox potentials (Fig. 2b; Table 2).

Table 1. Spectroscopic properties

	Absorbance	Photoluminescence[a]	
Complex	λ_{max}/nm[b]	r.t., λ_{max} / nm (eV)[b]	85 K, λ_{max} / nm (eV)[c]
$[Ru(bpy)_3]^{2+}$	243, 286, 420[f], 450	622 (1.99)	581[d] (2.13), 629
$Ir(ppy)_3$	240, 281, 373	520 (2.38)	494[e] (2.51) 531, 578[f]
$[Ir(df\text{-}ppy)_2(ptb)]^+$	245, 302[f], 359	453 (2.74), 483	448 (2.77), 480, 506, 516
$[Ir(df\text{-}ppy\text{-}CF_3)_2(ptb)]^+$	249, 266, 302[f], 376, 405[f]	470 (2.64), 495	460 (2.70), 493, 528[f]

[a]Corrected for the change in instrument sensitivity across the wavelength range (Fig. S1). The correction factor was established by using a light source with standard spectral irradiance. [b]10 μM in ACN. [c]5 μM in 4:1 (v/v) EtOH-MeOH. [d]Values obtained at 77 K include 580 nm by our group,[19] and Kawanishi *et al*.,[20] and 582 nm by Juris *et al*.,[21] and Nakamaru.[22] [e]Our group[19] and Dedeian *et al*.[23] reported a λ_{max} of 494 nm for $Ir(ppy)_3$ in EtOH-MeOH glasses at 77 K. [f]Shoulder

Table 2. MO energies and electrochemical potentials.

	Calculated MO energies (BP86/def2-TZVP)		Potentials[a] / V *vs* $Fc^{0/+}$	
Complex	HOMO /eV	LUMO /eV	M/M^+	M^-/M
$[Ru(bpy)_3]^{2+}$	-5.046	-3.278	0.89	-1.73, -1.92, -2.15
$Ir(ppy)_3$	-4.622	-2.303	0.33	-2.67
$[Ir(df\text{-}ppy)_2(ptb)]^+$	-5.309	-2.818	1.18	-2.12
$[Ir(df\text{-}ppy\text{-}CF_3)_2(ptb)]^+$	-5.432	-3.013	1.35 (1.30)[e]	-1.88 (-1.93)[b]
$[Ir(df(CF_3)\text{-}ppy\text{-}Me)_2(ptb)]^+$	-5.498	-2.836	(1.37)[e]	(-2.10)[b]
$[Ir(df(CN)\text{-}ppy)_2(ptb)]^+$	-5.654	-2.929	(1.53)[e]	(-2.01)[b]

[a]Cyclic voltammetry; electrodes: glassy carbon working, silver wire reference, platinum wire counter; 0.2 mM metal complex in dry ACN with 0.1 M $TBAPF_6$; solution degassed for 15 min prior to analysis; scan rate: 0.1 V s^{-1}. [b]Predicted from the difference in LUMO energies from those of the $[Ir(df\text{-}ppy)_2(ptb)]^+$ complex. The MO energies for all metal complexes discussed in this study are shown in Fig. S12.

Due to the strong σ-donation of its Ir-C bonds, the $Ir(ppy)_3$ complex (exhibiting a mixed metal-ligand HOMO and a ligand-based LUMO) is readily oxidised but difficult to reduce.[24] The introduction of the electron-withdrawing fluoro substituents on the phenyl rings stabilises the HOMO and to a lesser extent, the LUMO energy level. This results in a positive shift in the reduction potential and to a lesser extent, the oxidation potential, and a hypsochromic shift in the emission, without significant change to the quantum yield (0.99).[25, 26] The replacement of one df-ppy ligand in $Ir(df\text{-}ppy)_3$ with the substituted triazolylpyridine ligand (ptb) results in even greater MO stabilisation, more positive redox potentials, and a further blue-shift in luminescence.[26-29] Despite its lower photoluminescence quantum yield (0.21),[26, 27] $[Ir(df\text{-}ppy)_2(ptb)]^+$ produces more intense co-reactant ECL with TPrA[26] and several close analogues have been reported to exhibit greater annihilation ECL efficiencies[28] than $Ir(ppy)_3$.

Although $[Ir(df\text{-}ppy)_2(ptb)]^+$ is reduced at a much less negative potential than that of $Ir(ppy)_3$ (Fig. 2b), the reaction of $[Ir(df\text{-}ppy)_2(ptb)]^0$ and $Ir(ppy)_3^+$ should still generate $Ir(ppy)_3$* (Equation 10), based on: (i) an estimation of reaction exergonicity comparing the redox potentials with the excited MLCT state energy;[14] (ii) the similarity of the $[Ir(df\text{-}ppy)_2(ptb)]^{+/0}$ couple (-2.12 V *vs* $Fc^{+/0}$) with $[Ru(bpy)_3]^{0/-}$ (-2.15 V *vs* $Fc^{+/0}$), which we previously observed as the least negative redox couple of the ruthenium complex that was capable of eliciting the $Ir(ppy)_3$* excited state upon reaction with $[Ir(ppy)_3]^+$ (Equation 7); and (iii) the cut-off reduction potential (approximately -2.10 V *vs* $Fc^{+/0}$) for efficient mixed ECL from organic nitriles/ketones with $Ir(ppy)_3$ reported by Kapturkiewicz and Angulo.[4] The feasibility of this reaction is supported by comparison of the calculated $[Ir(df\text{-}ppy)_2(ptb)]^0$ SOMO and $[Ir(ppy)_3]^+$ LUMO energies (Fig. 4a).

$$[Ir(ppy)_3]^+ + [Ir(df\text{-}ppy)_2(ptb)]^0 \rightarrow Ir(ppy)_3^* + [Ir(df\text{-}ppy)_2(ptb)]^+ \quad (10)$$

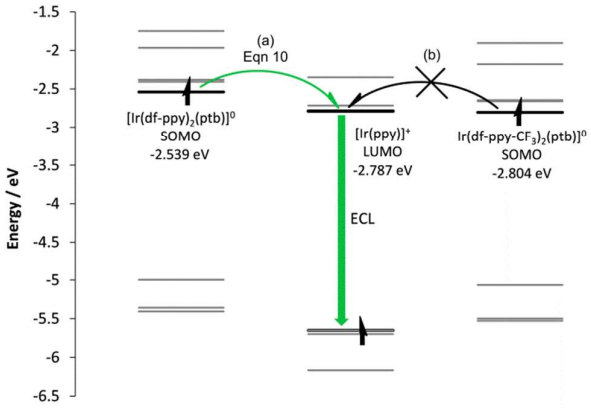

Figure 4. MO energies of $[Ir(df\text{-}ppy)_2(ptb)]^0$, $[Ir(df\text{-}ppy\text{-}CF_3)_2(ptb)]^0$ and $[Ir(ppy)_3]^+$, relevant to generation of $Ir(ppy)_3$*. The MO energies for all metal complexes discussed in this study are shown in Fig. S12.

We examined the annihilation ECL from mixtures of $[Ir(df\text{-}ppy)_2(ptb)]^+$ and $Ir(ppy)_3$ at various concentrations (in acetonitrile with 0.1 $TBAPF_6$) using alternating electrochemical potentials: one sufficient to oxidise only $Ir(ppy)_3$ or both complexes, and the other sufficient to reduce only $[Ir(df\text{-}ppy)_2(ptb)]^+$ or both complexes, thus giving four sets of applied potentials (Expt (i)-(iv) shown in Fig 5a).

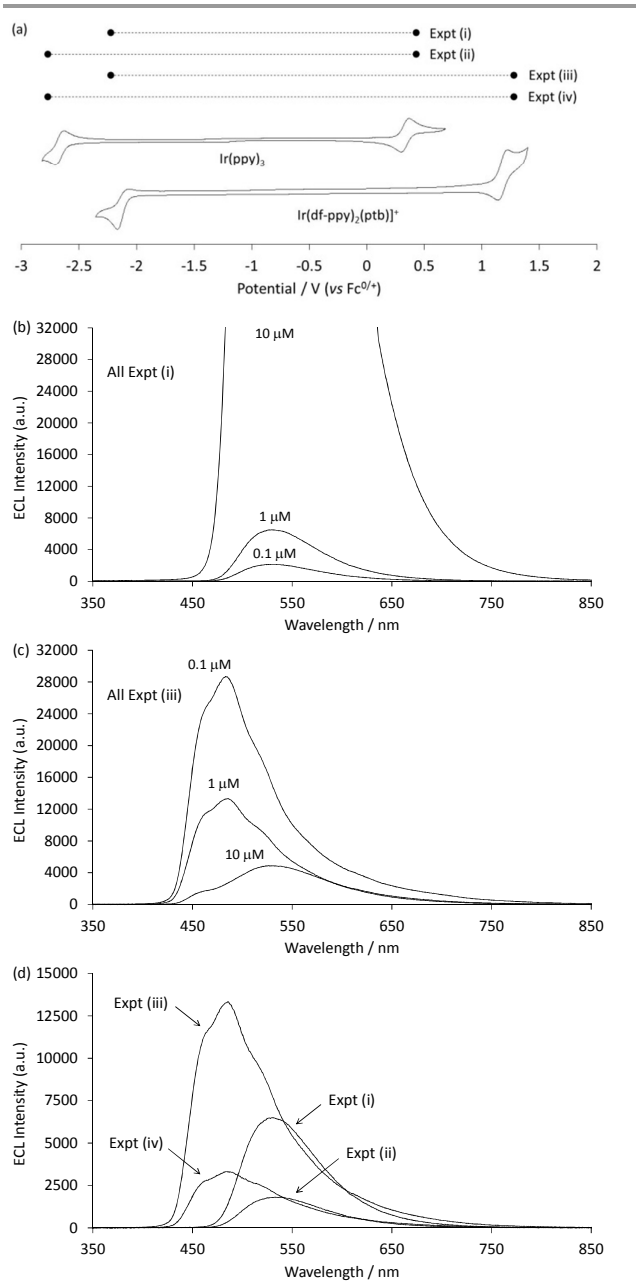

Figure 5. (a) An illustration of the four different sets of potentials applied to the mixture of $Ir(ppy)_3$ and $[Ir(df\text{-}ppy)_2(ptb)]^+$ (Expts (i)-(iv)), with cyclic voltammograms of the two Ir(III) complexes shown beneath. (b,c) ECL spectra for a mixture of 0.2 mM $[Ir(df\text{-}ppy)_2(ptb)]^+$ and varying concentrations (0.1, 1 and 10 μM) of $Ir(ppy)_3$ using (b) Expt (i) or (c) Expt (iii). (d) ECL spectra for a mixture of 0.2 mM $[Ir(df\text{-}ppy)_2(ptb)]^+$ and 1 μM $Ir(ppy)_3$, using each of the four sets of applied potentials (Expt (i)-(iv)). In each case, the two-step potential was applied at 10 Hz for 12 s. The lower structural detail in the emission from $[Ir(df\text{-}ppy)_2(ptb)]^+$ here compared to the photoluminescence emission shown in Fig. 2a is due to the lower spectral resolution of the instrumentation used to collect ECL spectra. In Fig. 5b, the ECL intensity at 10 μM $Ir(ppy)_3$ was 28-fold greater than at 1 μM.

In Expt (i), in which only $Ir(ppy)_3$ was oxidised and only $[Ir(df\text{-}ppy)_2(ptb)]^+$ was reduced, the spectral distribution matched that of the $Ir(ppy)_3$* emission, with no detectable contribution from $[Ir(df\text{-}ppy)_2(ptb)]^+$* (Fig. 5b). The ECL from this system increased in intensity with greater concentrations of $Ir(ppy)_3$ and/or $[Ir(df\text{-}ppy)_2(ptb)]^+$ (up to at least the highest concentration examined, 0.2 mM). This had two useful consequences: firstly, in the presence of 0.2 mM $[Ir(df\text{-}ppy)_2(ptb)]^+$, the $Ir(ppy)_3$ complex could be detected down to nanomolar levels – many orders of magnitude below what could be observed by the annihilation ECL of $Ir(ppy)_3$ (in the absence of $[Ir(df\text{-}ppy)_2(ptb)]^+$) with this instrumental configuration. Secondly, the intensity of the mixed annihilation ECL between high concentrations of $Ir(ppy)_3$ and $[Ir(df\text{-}ppy)_2(ptb)]^+$ far exceeded the maximum intensity of the annihilation ECL of $Ir(ppy)_3$, which is limited by its solubility in acetonitrile. The ECL of a mixture of 0.2 mM $Ir(ppy)_3$ and 0.2 mM $[Ir(df\text{-}ppy)_2(ptb)]^+$ exhibited an intensity that was ~19-fold greater than the annihilation ECL of 0.2 mM $Ir(ppy)_3$ alone. We attribute this in part to species available at the electrode surface during the alternating electrochemical potentials. When the reductive potential is applied in the mixed system, there is a supply of $[Ir(df\text{-}ppy)_2(ptb)]^+$ that was not oxidised in the previous pulse.

Similarly, when the oxidative potential is applied, there is a pool of $Ir(ppy)_3$ that was inert to the previous reductive pulse. Moreover, the mixed system exhibited greater annihilation ECL efficiency (by 2.9-fold at a concentration of 0.1 mM). This is consistent with Kapturkiewicz and Angulo's observation that the mixed annihilation ECL of $Ir(ppy)_3^{0/+}$ with the radical anions of aromatic nitriles and ketones (where the ΔG_{es} was between ~0 and -0.36 eV) exhibited greater ECL efficiencies than the annihilation ECL of $Ir(ppy)_3$ alone (ΔG_{es} -0.51 eV),[4] where the reduced efficiency was tentatively attributed to additional parasitic processes occurring at the large negative potentials required for the reduction of $Ir(ppy)_3$.

If we repeat the above experiment, but move the reductive pulse further negative, so that both $[Ir(df\text{-}ppy)_2(ptb)]^+$ and $Ir(ppy)_3$ are reduced (Fig. 5a, Expt (ii)), there are now two pathways to the $Ir(ppy)_3$* emitter (Equations 10 and 9). The application of this wider potential range, however, diminishes the ECL intensity (for example, compare plots (i) and (ii) in Fig. 5d). This appears to arise from two factors: firstly, at potentials sufficiently negative to reduce $Ir(ppy)_3$, the $[Ir(df\text{-}ppy)_2(ptb)]^0$ species is subject to further irreversible reductions (Fig S3a, blue plot). Secondly, the applied reductive potential nears the edge of the potential window, inviting deleterious reactions with the solvent, particularly if traces of water are present. This may play a role in the greater efficiency of the mixed ECL system (Equation 10) compared to the annihilation ECL of $Ir(ppy)_3$ in the absence of $[Ir(df\text{-}ppy)_2(ptb)]^+$ as described above.

In Expt (iii), in which appropriate potentials were applied to oxidise *both* $Ir(ppy)_3$ and $[Ir(df\text{-}ppy)_2(ptb)]^+$, but reduce only $[Ir(df\text{-}ppy)_2(ptb)]^+$, the spectral distribution of the resulting ECL can comprise contributions from both $Ir(ppy)_3$* (Equation 10) and $[Ir(df\text{-}ppy)_2(ptb)]^+$* (Equation 11). The ratio of these contributions was highly dependent on the concentrations of the two complexes (Fig. 5c and S6). There is considerable overlap between the luminescence of $Ir(ppy)_3$ and $[Ir(df\text{-}ppy)_2(ptb)]^+$, but their relative contributions to the ECL can be readily quantified by deconvolution of the overall emission into their characteristic spectra (Fig. S4).[16] In a few cases, there was some deviation from the model, particularly on the longer wavelength side of the emission, which we attribute to the overlap of the shorter wavelengths of the $[Ir(df\text{-}ppy)_2(ptb)]^+$ emission with the lowest energy absorption bands of $Ir(ppy)_3$ (Fig. S5a) and/or an unexpected subsequent oxidation of $Ir(ppy)_3$ at the high applied potential required to oxidise the $[Ir(df\text{-}ppy)_2(ptb)]^+$ complex (Fig. S3a, green plot).

$$[Ir(df\text{-}ppy)_2(ptb)]^{2+} + [Ir(df\text{-}ppy)_2(ptb)]^0 \rightarrow [Ir(df\text{-}ppy)_2(ptb)]^+* + [Ir(df\text{-}ppy)_2(ptb)]^+ \quad (11)$$

When these potentials are applied to this mixed ECL system, it can be thought of as the annihilation ECL of $[Ir(df\text{-}ppy)_2(ptb)]^+$, quenched by the presence of $Ir(ppy)_3$ (Fig. 5c and S6). Using a mixture of 200 μM $[Ir(df\text{-}ppy)_2(ptb)]^+$ and 0.1 μM $Ir(ppy)_3$, the contribution of $Ir(ppy)_3$* to the emission was less than 0.01%. However, with $Ir(ppy)_3$ at 1 μM and 10 μM, the contribution of $Ir(ppy)_3$* to the emission increased to 5.3% and 70.6%, and the overall emission intensity (integrated area) decreased by 2.1-fold and 4.8-fold, respectively. The efficient quenching of the ECL from $[Ir(df\text{-}ppy)_2(ptb)]^+$ in this mixed system most likely results from several processes, including electron transfers between ground and/or excited states (Equations 10, 12 and 13 and processes involving the further oxidation of $Ir(ppy)_3$, Fig. S3a, green plot) and direct energy transfer (Equation 14; Fig. S5a).

$$[Ir(df\text{-}ppy)_2(ptb)]^{2+} + Ir(ppy)_3 \rightarrow [Ir(df\text{-}ppy)_2(ptb)]^+ + Ir(ppy)_3^+ \quad (12)$$

$$[Ir(df\text{-}ppy)_2(ptb)]^+* + Ir(ppy)_3 \rightarrow [Ir(df\text{-}ppy)_2(ptb)]^0 + Ir(ppy)_3^+ \quad (13)$$

$$[Ir(df\text{-}ppy)_2(ptb)]^+* + Ir(ppy)_3 \rightarrow [Ir(df\text{-}ppy)_2(ptb)]^+ + Ir(ppy)_3* \quad (14)$$

To complete this series of experiments, we applied alternating potentials sufficient to both oxidise and reduce both complexes (Fig. 5a, Expt (iv)). Similar to that described above, extending the potential range to include the reduction of $Ir(ppy)_3$ resulted in a decrease in ECL intensity (for example, compare plots (iii) and (iv) in Fig. 5d). In this case, where both luminophores can contribute to the emission, the reduction of $Ir(ppy)_3$ also increased its relative contribution to the emission.

Manipulating the redox potentials to switch off the cross-complex excitation

In all annihilation ECL involving mixtures of metal complexes reported to date, the application of the lowest anodic and cathodic potentials required for only the most facile oxidation and reduction still produced species capable of generating the lower energy excited state of the luminophores. In the novel system described above, this comprised the oxidation of $Ir(ppy)_3$ and reduction of $[Ir(df\text{-}ppy)_2(ptb)]^+$ (Expt (i) in Fig. 5a) to form species that react with sufficient energy to generate

the characteristic green ECL from $Ir(ppy)_3$* (Equation 10). In that case, however, the reduction potential of $[Ir(df\text{-}ppy)_2(ptb)]^+$ is only sufficient by 20-180 mV.[4, 14] We therefore sought to eliminate that pathway to generate the $Ir(ppy)_3$* emitter through a subtle modification of the $[Ir(df\text{-}ppy)_2(ptb)]^+$ structure that would stabilise the LUMO energy level.

The frontier MO character of $[Ir(C^N)_2(N^N)]^+$ complexes in which C^N is ppy or df-ppy, and N^N is a 1-substituted 1,2,3-triazol-4-ylpyridine (Fig. 6a)[26, 29, 30] is generally akin to analogous complexes in which N^N is a more commonly employed bipyridine-type ligand (Fig. 6b).[31-33] In these complexes, the HOMO is an admixture of the metal-centred dπ orbitals and phenyl π orbitals of the C^N ligands and the LUMO is normally associated with the neutral N^N ancillary ligand. A change in reduction potential, as is desired in our study, is therefore often achieved through manipulation of the ancillary ligand. Implementing a less negative reduction potential in that manner would also induce a considerable bathochromic shift in the luminescence, and lessen the desired distinction with $Ir(ppy)_3$.

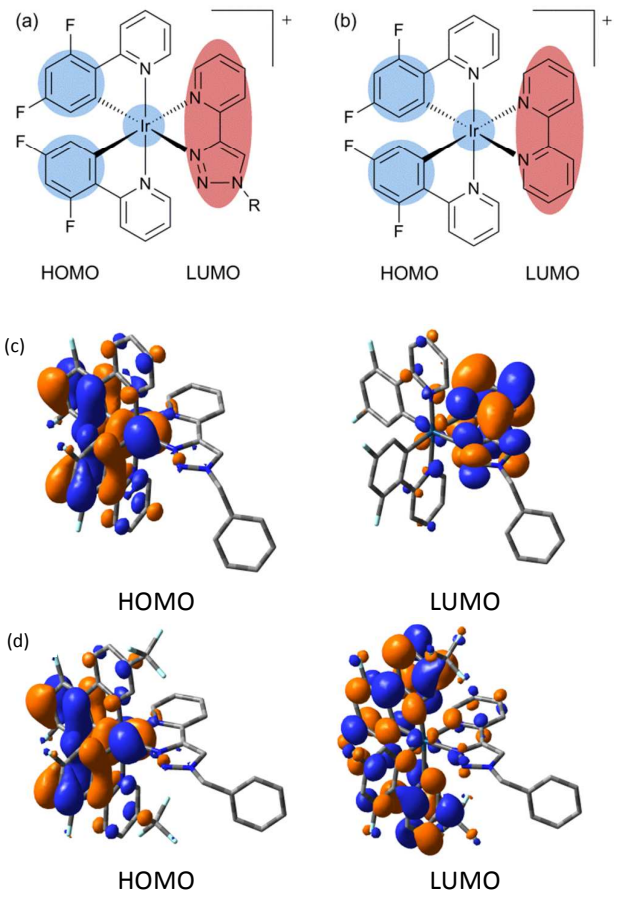

Figure 6. (a,b) Simplified depiction of the spatial distribution of HOMO and LUMO typically calculated for $[Ir(C^N)_2(N^N)]^+$ complexes, where C^N is ppy, df-ppy or related ligands, and N^N is (a) a triazolylpyridine or (b) a bipyridine type ligand. (c,d) BP86/def2-TZVP ground-state frontier molecular orbital contour plots for (c) $[Ir(df\text{-}ppy)_2(ptb)]^+$ and (d) $[Ir(df\text{-}ppy\text{-}CF_3)_2(ptb)]^+$. Additional contour plots are shown in Fig. S10.

Despite the spatial separation of the frontier MOs of these complexes, manipulation of oxidation and reduction potentials is not entirely orthogonal. And whilst addition of further electron withdrawing groups to the df-ppy ligands could be anticipated to have a greater effect on the oxidation potential, it could also provide a sufficient change to the reduction potential for our purposes, without a large, deleterious bathochromic shift to the emission. With this approach, the novel analogue could potentially be prepared from one of several commercially available dimeric ($[Ir(C^N))_2(\mu\text{-}Cl)]_2$) precursors, where C^N is one of the three df-ppy derivatives shown in Fig. 7.

None of the three proposed complexes had previously been prepared, but the calculated LUMO energies of the complexes predicted a change in reduction potential (relative to $[Ir(df\text{-}ppy)_2(ptb)]^+$) of +18 mV for $[Ir(df(CF_3)\text{-}ppy\text{-}Me)_2(ptb)]^+$, +111 mV for $[Ir(df(CN)\text{-}ppy)_2(ptb)]^+$ and +195 mV for $[Ir(df\text{-}ppy\text{-}CF_3)_2(ptb)]^+$ (Table 2). Moreover, calculation of SOMO energies for the reduced complexes, $[Ir(df\text{-}ppy)_2(ptb)]^0$ (-2.539 eV), $[Ir(df(CF_3)\text{-}ppy\text{-}Me)_2(ptb)]^0$ (-2.583 eV), $[Ir(df(CN)\text{-}ppy)_2(ptb)]^0$ (-2.723 eV) and $[Ir(df\text{-}ppy\text{-}CF_3)_2(ptb)]^+$ (-2.804 eV) showed that only the SOMO of $[Ir(df\text{-}ppy\text{-}CF_3)_2(ptb)]^+$ was lower in energy than the LUMO of $[Ir(ppy)_3]^+$ (-2.787 eV) (Fig. 4b and S12).

For the two complexes with the additional electron withdrawing substituent on the phenyl ring of df-ppy (associated with the HOMO), relatively large shifts in oxidation potential were anticipated, resulting in hypsochromic shifts in the emission. The pyridyl ring is less commonly modified than the phenyl ring of the C^N ligand or the ancillary N^N ligand for electrochemical or spectroscopic modulation of $[Ir(C^N)_2(N^N)]^+$ complexes,[34] but the approach has found application, such as in the $[Ir(df\text{-}ppy\text{-}CF_3)_2(dtb\text{-}bpy)]^+$ complex (where dtb-bpy = 4,4'-di-*t*-butyl-2,2'-bipyridine), which is widely employed as a photoredox catalyst.[32, 35] The addition of CF_3 to the pyridyl moiety of the df-ppy ligands within $[Ir(df\text{-}ppy)_2(bpy)]^+$ and $[Ir(df\text{-}ppy)_2(dtb\text{-}bpy)]^+$ imparts a considerable hypsochromic shift in their luminescence,[36] but our calculations predict a small bathochromic shift upon addition of the CF_3 group to the same positions in the $[Ir(df\text{-}ppy)_2(ptb)]^+$ analogue.

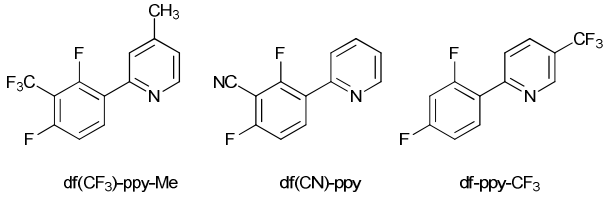

Figure 7. The C^N ligands within the three commercially available $[Ir(C^N))_2(\mu\text{-}Cl)]_2$ precursors that we considered for the preparation of an $[Ir(df\text{-}ppy)_2(ptb)]^+$ analogue with a less negative reduction potential.

We therefore chose to prepare the $[Ir(df\text{-}ppy\text{-}CF_3)_2(ptb)]^+$ complex (as the hexafluorophosphate salt), for which the predicted difference in the reduction potential from the parent $[Ir(df\text{-}ppy)_2(ptb)]^+$ was greater than that required (20-180 mV) to leave the reaction between the reduced complex and

$Ir(ppy)_3^+$ with insufficient energy to generate $Ir(ppy)_3$*. The novel $[Ir(df\text{-}ppy\text{-}CF_3)_2(ptb)](PF_6)$ was synthesised based on our previously reported procedure[26, 37] and characterised by multinuclear (^1H, ^{13}C, ^{19}F) homo- and heteronuclear NMR spectroscopy. High resolution mass spectrometry revealed a single molecular species corresponding to the cation $[Ir(df\text{-}ppy\text{-}CF_3)_2(ptb)]^+$, with its characteristic isotope pattern, in excellent agreement with the calculated *m/z* value. Crystals of $[Ir(df\text{-}ppy\text{-}CF_3)_2(ptb)](PF_6)$ suitable for single crystal X-ray crystallography were obtained and the solved structure revealed a distorted octahedral C_2N_4 environment around the central Ir(III) cation (Fig. 3c). The cyclometalating ligands were in a *N*,*N*-trans arrangement consistent with the geometry of the Ir(III) precursor. The ptb ligand occupied the final two coordination sites in a bidentate fashion, bound through the nitrogen of the pyridine ring and one nitrogen of the triazole heterocycle.

The changes in the reduction (+240 mV) and oxidation (+170 mV) potentials (Table 2) compared to $[Ir(df\text{-}ppy)_2(ptb)]^+$ were marginally higher than predicted, and a small bathochromic shift in the luminescence ($\Delta\lambda_{max}$ = +17 nm; Fig. 2a and Table 1) was observed, as anticipated. This might at first glance appear to contradict previous observations when the CF_3 group was introduced into the same position on the df-ppy ligands of related $[Ir(C\text{^}N)_2(N\text{^}N)]^+$ complexes such as $[Ir(df\text{-}ppy)_2(dtb\text{-}bpy)]^+$ ($\Delta E_{red} < \Delta E_{ox}$, $\Delta\lambda_{max}$ = −40 nm)[36], but the differences can be rationalised by considering the nature of their calculated MOs.[31, 38, 39] The frontier MOs of both $[Ir(df\text{-}ppy)_2(dtb\text{-}bpy)]^+$ and $[Ir(df\text{-}ppy\text{-}CF_3)_2(dtb\text{-}bpy)]^+$ are characterised by the general depiction for $[Ir(C\text{^}N)_2(N\text{^}N)]^+$ complexes shown in Fig. 6b. The CF_3 group exerts a strong stabilising effect on higher unoccupied MOs associated with the π* orbitals of the pyridine rings of the df-ppy ligands, but they remain above the N^N-ligand based LUMO.[31, 40] In this case, the greater influence on the oxidation than the reduction potential is a consequence of the greater stabilising effect of the CF_3 substituent on the π* orbitals of the phenyl ring on the same ligand (contributing to the HOMO), than on those of the ancillary N^N ligand (contributing to the LUMO). The lowest energy triplet of $[Ir(df\text{-}ppy)_2(dtb\text{-}bpy)]^+$ exhibits ^{3}MLCT/^{3}LLCT (HOMO→LUMO) character,[38] and the increase in the HOMO-LUMO gap is accompanied by a hypsochromic shift in the emission.

The $[Ir(df\text{-}ppy)_2(ptb)]^+$ complex also exhibits a N^N-ligand based LUMO (Fig. 6a and 6c), but it is considerably higher in energy than that of $[Ir(df\text{-}ppy)_2(dtb\text{-}bpy)]^+$, as seen in the difference in their reduction potentials of over 300 mV (Table S1). In this case, the stabilising effect of the CF_3 groups creates a new LUMO from one of the higher unoccupied MOs associated with the pyridine π* orbitals (Fig. 6d and S11). Based on the observed oxidation potentials (Table S1), the stabilisation of the HOMO is similar to that in the $[Ir(df\text{-}ppy\text{-}CF_3)_2(dtb\text{-}bpy)]^+$ complexes, but in the ptb analogue it is marginally outweighed by the decrease in LUMO energy, with a corresponding small bathochromic shift in the mixed ^{3}MLCT/^{3}LC emission. The emission spectra of $[Ir(df\text{-}ppy)_2(ptb)]^+$ and $[Ir(df\text{-}ppy\text{-}CF_3)_2(ptb)]^+$ show resolved vibronic structure (consistent with other $[Ir(C\text{^}N)_2(L)]^+$ complexes in which L is a 1,2,3-triazole ligand) due to some mixing between the ^{3}MLCT and ^{3}LC states.[27, 29, 30, 37, 41]

Upon application of alternating anodic and cathodic potentials at the working electrode that were sufficient to oxidise $Ir(ppy)_3$ and reduce $[Ir(df\text{-}ppy\text{-}CF_3)_2(ptb)]^+$ (Fig. 8a, Expt (v)), no significant ECL emission was observed (Fig. S9). By design, the subsequent reaction of the oxidised and reduced complexes is not sufficiently exergonic to generate the excited state $Ir(ppy)_3$* species (unlike Equation 10). Nevertheless, the 'dark' reaction to ground state products (Equation 15) can still occur.

$$[Ir(ppy)_3]^+ + [Ir(df\text{-}ppy\text{-}CF_3)_2(ptb)]^0 \rightarrow Ir(ppy)_3 + [Ir(df\text{-}ppy\text{-}CF_3)_2(ptb)]^+ \quad (15)$$

When we adjusted the oxidative pulse to a potential sufficient to oxidise both complexes (Fig. 8a, Expt (vii)) the annihilation ECL of $[Ir(df\text{-}ppy\text{-}CF_3)_2(ptb)]^+$ can occur (Equation 16).

$$[Ir(df\text{-}ppy\text{-}CF_3)_2(ptb)]^{2+} + [Ir(df\text{-}ppy\text{-}CF_3)_2(ptb)]^0 \rightarrow [Ir(df\text{-}ppy\text{-}CF_3)_2(ptb)]^+* + [Ir(df\text{-}ppy\text{-}CF_3)_2(ptb)]^+ \quad (16)$$

The annihilation ECL of $[Ir(df\text{-}ppy\text{-}CF_3)_2(ptb)]^+$ was quenched by $Ir(ppy)_3$ (Fig. 8b) even more efficiently than that of $[Ir(df\text{-}ppy)_2(ptb)]^+$ (Fig. 5c and S8). Bearing in mind the similarities in their spectroscopic and electrochemical properties, we assume the same processes for quenching espoused for the annihilation of $[Ir(df\text{-}ppy)_2(ptb)]^+$ operate in this case, except that the reaction between the mixed oxidised and reduced species can only lead to the ground state product (Equation 15). Considering the absence of a significant contribution from $Ir(ppy)_3$* to the ECL of this system (Fig. 8b), we conclude that the observed contribution from $Ir(ppy)_3$* in the analogous ECL from the $Ir(ppy)_3$-$[Ir(df\text{-}ppy)_2(ptb)]^+$ system (Fig. 5c) predominantly arose from electron transfer (Equation 10) rather than energy transfer (Equation 14) (although we acknowledge that the overlap between the emission of $[Ir(df\text{-}ppy\text{-}CF_3)_2(ptb)]^+$ with the absorption bands of $Ir(ppy)_3$ (Fig. S7a) is slightly lower than that of $[Ir(df\text{-}ppy)_2(ptb)]^+$ (Fig. S5a)).

If we instead apply alternating potentials suitable for the annihilation ECL of $Ir(ppy)_3$ (Expt (vi)), both complexes will be reduced, but only $Ir(ppy)_3$ will be oxidised. Similar to the quenching of the annihilation ECL of $[Ir(df\text{-}ppy\text{-}CF_3)_2(ptb)]^+$ in the presence of the $Ir(ppy)_3$ described above, the annihilation ECL of $Ir(ppy)_3$ was effectively quenched by the presence of $[Ir(df\text{-}ppy\text{-}CF_3)_2(ptb)]^+$ (Fig. 8c), which in this case can be attributed to a combination of the mixed dark reactions (Equations 15 and 17), including those involving the further reduction of $[Ir(df\text{-}ppy\text{-}CF_3)_2(ptb)]^0$ (Fig. S3b) (*e.g.*, Equation 18) and oxidative quenching of $Ir(ppy)_3$* (Equation 19).

$$[Ir(df\text{-}ppy\text{-}CF_3)_2(ptb)]^+ + [Ir(ppy)_3]^- \rightarrow [Ir(df\text{-}ppy\text{-}CF_3)_2(ptb)]^0 + Ir(ppy)_3 \quad (17)$$

$$[Ir(df\text{-}ppy\text{-}CF_3)_2(ptb)]^0 + [Ir(ppy)_3]^- \rightarrow [Ir(df\text{-}ppy\text{-}CF_3)_2(ptb)]^- + Ir(ppy)_3 \quad (18)$$

$$[Ir(df\text{-}ppy\text{-}CF_3)_2(ptb)]^+ + Ir(ppy)_3* \rightarrow [Ir(df\text{-}ppy\text{-}CF_3)_2(ptb)]^0 + [Ir(ppy)_3]^+ \quad (19)$$

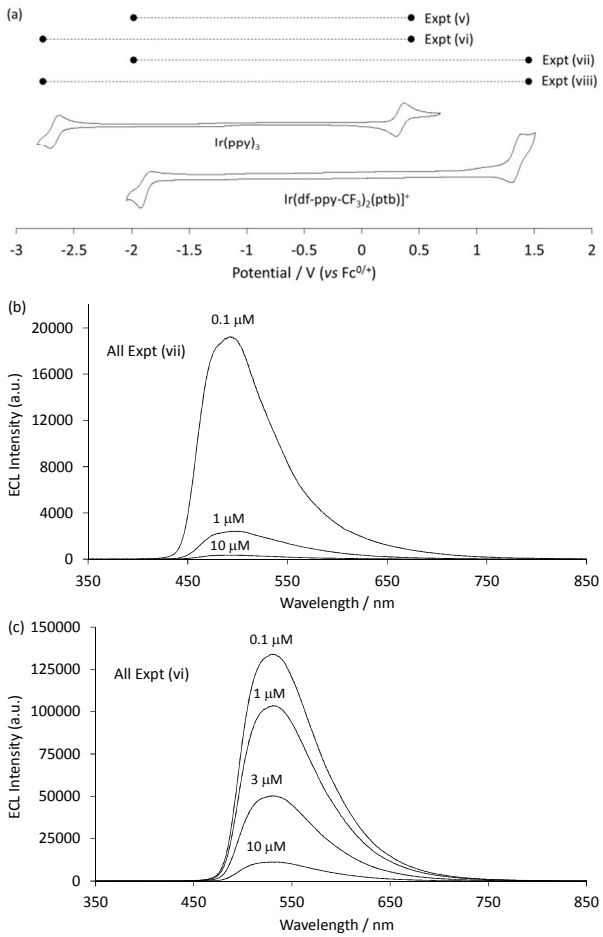

Figure 8. (a) An illustration of the four different sets of potentials applied to the mixture of $Ir(ppy)_3$ and $[Ir(df\text{-}ppy\text{-}CF_3)_2(ptb)]^+$ (Expts (v)-(viii)), with cyclic voltammograms of the two individual Ir(III) complexes shown beneath. (b) ECL spectra for a mixture of 0.2 mM $[Ir(df\text{-}ppy\text{-}CF_2)_2(ptb)]^+$ and 0.1, 1 or 10 μM $Ir(ppy)_3$, using Expt (vii), in which the alternating applied potentials were sufficient to oxidise both complexes, but reduce only $[Ir(df\text{-}ppy\text{-}CF_3)_2(ptb)]^+$. (c) ECL spectra for a mixture of 0.2 mM $Ir(ppy)_3$ and 0.1, 1, 3 or 10 μM $[Ir(df\text{-}ppy\text{-}CF_2)_2(ptb)]^+$, using Expt (vi), in which the applied alternating potentials were sufficient to oxidise only $Ir(ppy)_3$ and reduce both complexes. In each case, the two-step potential was applied at 10 Hz for 12 s. The lower structural detail in the emission from $[Ir(df\text{-}ppy\text{-}CF_3)_2(ptb)]^+$ here compared to the photoluminescence emission shown in Fig. 2a is due to the lower spectral resolution of the instrumentation used to collect ECL spectra.

Conclusions

The two cases presented in this study and the previously discussed[14, 16] $Ir(ppy)_3$-$[Ru(bpy)_3]^{2+}$ system represent three distinct outcomes of ECL reactions between the electrochemically oxidised $Ir(ppy)_3^+$ and the first reduction product of another electrochemiluminophore (Fig. 2b). In the reaction with $[Ru(bpy)_3]^+$, there is insufficient free energy to attain $Ir(ppy)_3$*, but the lower energy $[Ru(bpy)_3]^{2+}$* is populated (Equation 3). Conversely, in the reaction with $[Ir(df\text{-}ppy)_2(ptb)]^0$, $Ir(ppy)_3$* is formed, but $[Ir(df\text{-}ppy)_2(ptb)]^+$* is not (Equation 10). With $[Ir(df\text{-}ppy\text{-}CF_3)_2(ptb)]^0$, there is insufficient energy to attain either excited state (Equation 15). As demonstrated herein, this approach possesses several advantages over conventional annihilation ECL involving comproportionation reactions. The combination of two electroactive species enables one to be detected at exceeding low concentrations when the other is in excess. Moreover, it could improve the operational parameters of simple ECL-based light-emitting devices[13, 42] across a range of visible emission colours, including lower operating power (for example, the mixed annihilation ECL of $Ir(ppy)_3$ and $[Ir(df\text{-}ppy)_2(ptb)]^+$ has an ΔE of 2.45 eV compared to 3.00 eV for the annihilation ECL of $Ir(ppy)_3$ alone), greater ECL efficiencies (by avoiding parasitic reactions at extreme potentials) and greater overall emission intensities than either individual annihilation ECL system. Within these devices, however, the solubility of the luminophores within the matrix must also be optimised.

One remaining outcome of an ECL reaction between the electrochemically oxidised $Ir(ppy)_3^+$ and the first reduction product of another electrochemiluminophore, which was not included here, is where there is sufficient energy to attain the excited state of either electrochemiluminophore. This would require two luminophores with a similar difference between their first oxidation and first reduction potentials (ΔE) and therefore comparable emission colour. In that case, the dominant emitter from the electrochemiluminophores may also be influenced by differences in their luminescence quantum yield and/or the kinetic advantage of ligand-to-ligand electron transfer (where the electrochemically oxidised electron-accepting luminophore is excited) over metal-to-metal electron transfer (where the electrochemically reduced electron-donating luminophore is excited).[43]

If we apply potentials beyond the first oxidation and first reduction of either complex, then there are of course other combinations of species for which the free energy of their reaction exceeds that required to generate either excited state (for example, the reaction of $Ir(ppy)_3^-$ and $[Ir(df\text{-}ppy)_2(ptb)]^{2+}$ formed in Expt (ii), Fig. 5a). These species, however, cannot be generated in isolation from the more facile oxidation and/or reduction products (which are $Ir(ppy)_3^+$ and $[Ir(df\text{-}ppy)_2(ptb)]^0$ in the above example), and their reactions are vulnerable to other interferences as described in the previous section. Generally, electron transfer at anodic and cathodic potentials beyond the first oxidation of the most easily oxidised luminophore and the first reduction of the most easily reduced luminophore initiates multiple competing annihilation ECL reactions. In both the $Ir(ppy)_3$-$[Ir(df\text{-}ppy)_2(ptb)]^+$ and the $Ir(ppy)_3$-$[Ru(bpy)_3]^{2+}$ systems, and the large difference in the energy of the electronically excited states of the two luminophores appears to be the dominant factor in the relative emission intensities. In both systems, an excess in the concentration of the higher energy luminophore can be used to balance the intensities, so that the dominant emitter can be determined through the selection of applied potentials to manipulate the species generated at the electrode surface (*e.g.*, Fig. 5d).

The ability to eliminate the efficient annihilation ECL from the $Ir(ppy)_3$-$[Ir(df\text{-}ppy)_2(ptb)]^+$ system through subtle change in ligand structure highlights the ease in which these light-producing reactions can be manipulated, considering simple

estimations of reaction exergonicity and DFT-modelling based predictions of reduction and oxidation potentials. The absence of ECL from the reaction of $Ir(ppy)_3^+$ and $[Ir(df\text{-}ppy\text{-}CF_3)_2(ptb)]^0$ removes its contribution to the ECL of either comproportionation reaction (Equations 9 and 16), but in this particular combination, the generation of either excited state is subject to parasitic processes that result in ECL that is much less intense than that observed in the absence of the other luminophore.

Experimental

Chemicals

Tris(2,2'-bipyridine)ruthenium(II) hexafluorophosphate ($[Ru(bpy)_3](PF_6)_2$), tetrabutylammonium hexafluorophosphate ($TBAPF_6$; electrochemical grade) and dichlorotetrakis[3,5-difluoro-2-(2-pyridinyl)phenyl]diiridium(III) ($[Ir(df\text{-}ppy)_2(\mu\text{-}Cl)]_2$) were purchased from Sigma-Aldrich (NSW, Australia). The other Ir(III) dimer (di-μ-chlorotetrakis[3,5-difluoro-2-[5-trifluoromethyl-2-pyridinyl-κN)phenyl-κC]diiridium(III); $[Ir(df\text{-}ppy\text{-}CF_3))_2(\mu\text{-}Cl)]_2$) and bis(cyclopentadienyl)iron (ferrocene), were purchased from Strem Chemicals (MA, USA). *fac*-Tris(2-phenylpyridine)iridium(III) ($Ir(ppy)_3$) was from Rubipy Scientific (ON, Canada). Potassium chloride for reference electrode storage was obtained from Labserv Pronalys (Vic., Australia). Acetonitrile was from Scharlau (Barcelona, Spain) and was distilled over calcium hydride under a nitrogen atmosphere and collected as needed. Solutions were degassed using argon or nitrogen for approximately 15 minutes prior to analysis.

NMR spectra were acquired on a Bruker Biospin AV400 spectrometer. ^1H NMR spectra were acquired at 400 MHz, $^{13}C\{^1H\}$ NMR spectra were acquired at 100 MHz, and ^{19}F NMR acquired at 376 MHz. All NMR spectra were recorded at 298 K. Chemical shifts were referenced to residual solvent peaks and are quoted in terms of parts per million (ppm), relative to tetramethylsilane ($Si(CH_3)_4$); ^{19}F NMR signals are quoted relative to an internal standard of hexafluorobenzene.

$[Ir(df\text{-}ppy)_2(ptb)](PF_6)$: This complex was synthesised according to the previously published procedure.[26, 37] The ^1H NMR spectrum (Fig. S13) was consistent with the literature values. ^1H NMR (400 MHz; $CDCl_3$): δ 8.80 (1H, s, ptb-triazolyl-*H*), 8.30 (2H, t, J = 10.5 Hz, phenyl-*H*), 8.22 (1H, d, J = 7.9 Hz, ptb-pyridyl-*H*), 8.00 (1H, td, J = 7.9, 1.5 Hz, ptb-pyridyl-*H*), 7.79-7.83 (3H, m, pyridyl-*H*, ptb-pyridyl-*H*), 7.61 (1H, d, J = 5.8 Hz, pyridyl-*H*), 7.45 (1H, d, J = 5.8 Hz, pyridyl-*H*), 7.36 (5H, s, ptb-phenyl-*H*), 7.32 (1H, m, pyridyl-*H*), 7.11 (1H, ddd, J = 7.3, 5.9, 1.3 Hz, pyridyl-*H*), 7.01 (1H, ddd, J = 7.3, 5.9, 1.3 Hz, pyridyl-*H*), 6.55 (2H, m, phenyl-*H*), 5.73 (1H, dd, J = 8.5, 2.5 Hz, phenyl-*H*), 5.68 (1H, dd, J = 8.5, 2.3 Hz, phenyl-*H*), 5.58 (2H, s, triazole−CH_2−phenyl). ESI-MS (positive ion). Calcd for $C_{36}H_{24}F_4IrN_6^+$ ($[M]^+$): *m/z* 809.163. Found *m/z* 809.1638.

$[Ir(df\text{-}ppy\text{-}CF_3))_2(ptb)](PF_6)$: The dimer $[Ir(df\text{-}ppy\text{-}CF_3))_2(\mu\text{-}Cl)]_2$ (80 mg, 54 μmol) and 2-(1-(benzyl)-1H-1,2,3-triazol-4-yl)pyridine (ptb, 25 mg, 108 μmol) were suspended in a 3:1 mixture of dichloromethane and methanol. Starting materials typically solubilized within 1 h. Reactions were stirred in darkness under an inert atmosphere for 16 h. The solvents were then removed and the residue dissolved in acetonitrile and filtered through a filter aid (Celite). The solvent was then removed by evaporation under reduced pressure and the residue redissolved in a minimum amount of ethanol and filtered through filter aid (Celite). To this solution was added a saturated aqueous solution of ammonium hexafluorophosphate until precipitation of a brightly coloured solid began to occur. The mixture was stirred in the dark for 16 h, and the product was then collected by filtration and washed with water, cold ethanol, ether, and lastly pentane, and then dried *in vacuo* to yield the product as a pale yellow solid (103 mg, 88 %). ^1H NMR (400 MHz; CD_2Cl_2): δ 8.84 (1H, s, ptb-triazolyl-*H*), 8.48 (2H, m, pyridyl-*H*), 8.26 (1H, d, J = 8.0 Hz, ptb-pyridyl-*H*), 8.15 (1H, td, J = 7.9, 1.6 Hz, ptb-pyridyl-*H*), 8.08 (2H, d, J = 8.9 Hz, pyridyl-*H*), 7.86 (1H, d, J = 5.4 Hz, ptb-pyridyl-*H*), 7.74 (1H, s, pyridyl-*H*), 7.55 (1H, s, pyridyl-*H*), 7.32-7.49 (6H, m, ptb-pyridyl-*H*, ptb-phenyl-*H*), 6.61-6.73 (2H, m, phenyl-*H*), 5.78 (1H, dd, J = 8.2, 2.3 Hz, phenyl-*H*), 5.71 (1H, dd, J = 8.3, 2.4 Hz, phenyl-*H*), 5.69 (1H, d, J = 14.6 Hz, ptb-triazole-CH_2-phenyl), 5.58 (1H, d, J = 14.6 Hz, ptb-triazole-CH_2-phenyl). $^{13}C\{^1H\}$ NMR (376 MHz; CD_2Cl_2): δ 56.9, 100.1 (t, J = 26.7 Hz), 100.6 (t, J = 26.0 Hz), 114.9, 115.1, 122.3 (2C, q, J = 272.6 Hz)), 124.2 (d, J = 21.5 Hz), 124.3 (d, J = 20.9 Hz), 124.6, 126.4 (m), 126.7 (m), 127.2 (m), 127.4 (2C, m), 128.1, 128.8 (2C), 130.0 (3C), 133.4, 137.2 (2C), 141.7, 145.5 (q, J = 5.0 Hz), 146.4 (q, J = 5.3 Hz), 149.2, 149.5, 150.7 (d, J = 7.5 Hz), 151.0, 154.1 (d, J = 7.2 Hz), 162.4 (dd, J = 196.3, 12.9 Hz), 162.9 (dd, J = 224.1, 13.1 Hz), 165.0 (dd, J = 193.0, 13.1 Hz), 165.5 (dd, J = 221.7, 12.9 Hz), 168.2(d, J = 7.2 Hz), 168.8 (d, J = 7.2 Hz). ^{19}F NMR (376 MHz; CD_2Cl_2): δ -65.1 (s), -65.3 (s), -74.6 (d, J = 711.2 Hz), -104.6 (d, J = 12.5 Hz), -105.7 (d, J = 12.1 Hz), -108.3 (d, J = 12.5 Hz), 109.2 (d, J = 12.0 Hz). The NMR spectra are included in the ESI (Fig. S14-S16). ESI-MS (positive ion). Calcd for $C_{38}H_{22}F_{10}IrN_6^+$ ($[M]^+$): *m/z* 945.138. Found *m/z* 945.1391.

Crystals of $[Ir(df\text{-}ppy\text{-}CF_3)_2(ptb)](PF_6)$ were mounted in low temperature oil then flash cooled. Intensity data were collected at 130.0(1) K on an X-ray diffractometer with CCD detector using $Mo_{K\alpha}$ (λ = 0.71073 Å) radiation. The structure was solved by direct methods and difference Fourier synthesis.[44] Thermal ellipsoid plots were generated using the program ORTEP-3 integrated within the WINGX suite of programs.[45] Crystal data for $[Ir(df\text{-}ppy\text{-}CF_3)_2(ptb)](PF_6)$: $IrC_{39}H_{24}Cl_2F_{16}N_6P$; M = 1174.71; T = 130.0(1) K; λ = 0.71073 Å; triclinic; space group $P\bar{1}$; a = 11.9028(4) Å; b = 12.4757(4) Å; c = 14.8516(5) Å; α = 84.354(3)°; β = 77.044(3)°; γ = 75.399(3)°; V = 2077.80(13) $Å^3$; Z = 2; D_C = 1.878 mg M^{-3}; μ(Mo Kα) = 3.491 mm^{-1}; F(000) = 1140; crystal size 0.562 × 0.148 × 0.044 mm^3; 19183 reflections measured; 12063 independent reflections (R_{int} = 0.0293); the final R = 0.0439 [$I > 2\sigma(I)$]; $w_R(F^2)$ = 0.1119 (all data); GOOF = 1.032.

Absorption and Photoluminescence Emission Spectra

Absorption spectra were collected using Cary 300 Bio UV/Vis spectrophotometer (Agilent, Vic., Australia) with 1 cm path length Spectrosil Quartz fluorimeter cuvettes with screw-top caps (Starna, Vic., Australia). Room temperature

photoluminescence spectra were collected using a Cary Eclipse spectrofluorimeter (5 nm band pass, 1 nm data interval, PMT voltage: 800 V; Agilent) with the cuvettes noted above. Low temperature photoluminescence spectra were obtained using an OptistatDN Variable Temperature Liquid Nitrogen Cryostat (Oxford Instruments, U.K.), with custom-made quartz sample holder (Fig. S17). Room temperature and low temperature emission spectra were corrected for the change in instrument sensitivity across the wavelength range, using a correction factor established using a quartz halogen tungsten lamp of standard spectral irradiance.[46] The low temperature spectra were collected at 85 K to avoid damage to the spectroscopic cuvettes at/near 77 K observed during our previous study[19] and by others.[47] We found no significant difference in the λ_{max} for $[Ru(bpy)_3]^{2+}$ and $Ir(ppy)_3$ at 77 K and 85 K under our instrumental conditions (Fig. S2), and the values were in good agreement with those previously reported[19-23] for $[Ru(bpy)_3]^{2+}$ and $Ir(ppy)_3$ in ethanol-methanol glasses at 77 K.

Electrochemistry and ECL

The electrochemical cell comprised a cylindrical glass vessel with a flat base and custom-built Teflon lid[16] with holes to fit the electrodes (glassy carbon working (CH Instruments), platinum wire counter and silver wire reference), and ensure a consistent cell configuration. The cell was housed in a light-tight faraday cage. Potentials were applied using an Autolab PGSTAT204 or PGSTAT128N potentiostat (Metrohm Autolab B.V., Netherlands), and referenced *in situ* to the ferrocene/ferrocenium ($Fc^{0/+}$) couple (0.2 mM). Spectra were collected using an Ocean Optics QE65pro or QEpro CCD spectrometer *via* optical fibre (1.0 m length, 1.0 mm core diameter) and collimating lens (Ocean Optics 74-UV, 200–2000 nm), positioned directly under the working electrode. Freshly distilled acetonitrile with 0.1 M $TBAPF_6$ supporting electrolyte was used as the solvent. Prior to each experiment, each electrode was cleaned/polished. The working electrodes were polished using 0.3 mm and 0.05 mm alumina powder on a felt pad with deionised water. All electrodes were rinsed with acetonitrile or acetone and dried with either nitrogen or argon. The solvent was degassed with nitrogen or argon for 15 minutes. For sets of experiments in which the ECL intensity exceeded the range of the spectrometer under our normal conditions, the proportion of light reaching the spectrometer was lowered by reducing the entrance slit width. The ECL from multiple luminophores was deconvoluted into their characteristic spectral distributions using the Solver function of Microsoft Excel (*e.g.*, Fig. S4).[16]

Computational Methods

DFT calculations were carried out within the Gaussian 09 suite of programs.[48] Ground state singlet and triplet geometries were optimised in the presence of solvent with the BP86 functional[49] in conjunction with the def2-TZVP basis set and associated core potential.[50] For $Ir(ppy)_3$, the mPW1PW91 functional[51] was used as geometry optimisation with BP86/def2-TZVP proved problematic. The polarisable continuum model (PCM)[52] self-consistent reaction field (SCRF) was used to model solvent effects with Truhlar's SMD solvent model,[53] with a solvent of acetonitrile for consistency with the experimental system. Stationary points were characterised as minima by calculating the Hessian matrix analytically at the same level of theory. All structures are minima with no imaginary frequencies. Molecular orbitals were calculated at the BP86/def2-TZVP level of theory, which has previously been demonstrated to produce reliable results.[19, 26] Molecular orbital analysis was carried out with the QMForge program.[54]

Conflicts of interest

There are no conflicts to declare.

Acknowledgements

This work was funded by the Australian Research Council (DP160103046). EK was supported by an Australian Postgraduate Award Scholarship. LCS and LC were supported by Deakin University Postgraduate Scholarships. We thank A/Prof. Trevor Smith and Mr Les Gammel (The University of Melbourne) for the construction of the custom-made sample holders for low temperature spectroscopy. We acknowledge generous allocations of computing from La Trobe University, Intersect, and NCI.

Notes and references

1. A. Kapturkiewicz, *Anal. Bioanal. Chem.*, 2016, **408**, 7013-7033; Z. Liu, W. Qi and G. Xu, *Chem. Soc. Rev.*, 2015, **44**, 3117-3142; S. Laird and F. Hogan Conor, in *Iridium(III) in Optoelectronic and Photonics Applications*, ed. E. Zysman-Colman, John Wiley & Sons, Inc., Chichester, UK, 2017, pp. 359-414.
2. A. Fiorani, G. Valenti, E. Villani, M. Marcaccio, E. Rampazzo, L. Prodi and F. Paolucci, in *Luminescence in Electrochemistry*, eds. F. Misomandre and P. Audebert, Springer, Gewerbestrasse, Switzerland, 2017, pp. 293-326.
3. K. Nishimura, Y. Hamada, T. Tsujioka, K. Shibata and T. Fuyuki, *Jpn. J. Appl. Phys., Part 2*, 2001, **40**, L945-L947; E. M. Gross, N. R. Armstrong and R. M. Wightman, *J. Electrochem. Soc.*, 2002, **149**, E137-E142; A. Kapturkiewicz, T.-M. Chen, I. R. Laskar and J. Nowacki, *Electrochem. Commun.*, 2004, **6**, 827-831; J. I. Kim, I.-S. Shin, H. Kim and J.-K. Lee, *J. Am. Chem. Soc.*, 2005, **127**, 1614-1615.
4. A. Kapturkiewicz and G. Angulo, *Dalton Trans.*, 2003, 3907-3913.
5. D. Bruce and M. M. Richter, *Anal. Chem.*, 2002, **74**, 1340-1342.
6. B. D. Muegge and M. M. Richter, *Anal. Chem.*, 2004, **76**, 73-77; L. Dennany, T. E. Keyes and R. J. Forster, *Analyst*, 2008, **133**, 753-759.
7. E. H. Doeven, E. M. Zammit, G. J. Barbante, C. F. Hogan, N. W. Barnett and P. S. Francis, *Angew. Chem., Int. Ed.*, 2012, **51**, 4354-4357; M. Schmittel, Q. Shu and M. E. Cinar, *Dalton Trans.*, 2012, **41**, 6064-6068; S. Wang, L. Ge, Y.

Zhang, X. Song, N. Li, S. Ge and J. Yu, *Lab Chip*, 2012, **12**, 4489-4498; K. N. Swanick, S. Ladouceur, E. Zysman-Colman and Z. Ding, *Angew. Chem., Int. Ed.*, 2012, **51**, 11079-11082.

8. E. H. Doeven, G. J. Barbante, C. F. Hogan and P. S. Francis, *ChemPlusChem*, 2015, **80**, 456-470.
9. E. H. Doeven, E. M. Zammit, G. J. Barbante, P. S. Francis, N. W. Barnett and C. F. Hogan, *Chem. Sci.*, 2013, **4**, 977-982; E. H. Doeven, G. J. Barbante, E. Kerr, C. F. Hogan, J. A. Endler and P. S. Francis, *Anal. Chem.*, 2014, **86**, 2727-2732; G. J. Barbante, N. Kebede, C. M. Hindson, E. H. Doeven, E. M. Zammit, G. R. Hanson, C. F. Hogan and P. S. Francis, *Chem. Eur. J.*, 2014, **20**, 14026-14031; H. Gao, S. Xia, R. Zhang, Y. Zhao, W. Wang, Z. An and H. Qi, *J. Electroanal. Chem.*, 2015, **755**, 71-76; Y.-Z. Wang, C.-H. Xu, W. Zhao, Q.-Y. Guan, H.-Y. Chen and J.-J. Xu, *Anal. Chem.*, 2017, **89**, 8050-8056; H. Li, L. Bouffier, S. Arbault, A. Kuhn, C. F. Hogan and N. Sojic, *Electrochem. Commun.*, 2017, **77**, 10-13; H. Gao, Q. Dang, S. Xia, Y. Zhao, H. Qi, Q. Gao and C. Zhang, *Sens. Actuators, B*, 2017, **253**, 69-76; Y.-Z. Wang, S.-Y. Ji, H.-Y. Xu, W. Zhao, J.-J. Xu and H.-Y. Chen, *Anal. Chem.*, 2018, DOI: 10.1021/acs.analchem.1028b00014.
10. W. Sun, S. Sun, N. Jiang, H. Wang and X. Peng, *Organometallics*, 2015, **34**, 3385-3389; W. Sun, S. Sun, N. Jiang, L. Gao and G. Zheng, *J. Organomet. Chem.*, 2017, **846**, 367-371.
11. M. A. Haghighatbin, S.-C. Lo, P. L. Burn and C. F. Hogan, *Chem. Sci.*, 2016, **7**, 6974-6980.
12. S. Li, S. Wang, M. Yan, S. Ge, L. Ge, J. Yu and X. Song, *Sens. Actuators, B*, 2013, **183**, 488-495; F. Han, H. Jiang, D. Fang and D. Jiang, *Anal. Chem.*, 2014, **86**, 6896-6902; Y. Cheng, Y. Huang, J. Lei, L. Zhang and H. Ju, *Anal. Chem.*, 2014, **86**, 5158-5163; Y. He, J. Li and Y. Liu, *Anal. Chem.*, 2015, **87**, 9777-9785; J. Shu, Z. Han, T. Zheng, D. Du, G. Zou and H. Cui, *Anal. Chem.*, 2017, **89**, 12636-12640
13. H. C. Moon, T. P. Lodge and C. D. Frisbie, *J. Am. Chem. Soc.*, 2014, **136**, 3705-3712.
14. E. Kerr, E. H. Doeven, G. J. Barbante, C. F. Hogan, D. Bower, P. S. Donnelly, T. U. Connell and P. S. Francis, *Chem. Sci.*, 2015, **6**, 472-479.
15. K. N. Swanick, M. Sandroni, Z. Ding and E. Zysman-Colman, *Chem. Eur. J.*, 2015, **21**, 7435-7440.
16. E. Kerr, E. H. Doeven, G. J. Barbante, C. F. Hogan, D. J. Hayne, P. S. Donnelly and P. S. Francis, *Chem. Sci.*, 2016, **7**, 5271-5279.
17. L. C. Soulsby, D. J. Hayne, E. H. Doeven, L. Chen, C. F. Hogan, E. Kerr, J. L. Adcock and P. S. Francis, *ChemElectroChem*, 2018, **5**, 1543-1547.
18. A. Kapturkiewicz, *Chem. Phys. Lett.*, 1995, **236**, 389-394; A. Kapturkiewicz, *Adv. Electrochem. Sci. Eng.*, 1997, **5**, 1-60; G. J. Barbante, C. F. Hogan, D. J. D. Wilson, N. A. Lewcenko, F. M. Pfeffer, N. W. Barnett and P. S. Francis, *Analyst*, 2011, **136**, 1329-1338.
19. L. Chen, E. H. Doeven, D. J. D. Wilson, E. Kerr, D. J. Hayne, C. F. Hogan, W. Yang, T. T. Pham and P. S. Francis, *ChemElectroChem*, 2017, **4**, 1797-1808.
20. Y. Kawanishi, N. Kitamura and S. Tazuke, *Inorg. Chem.*, 1989, **28**, 2968-2975.
21. A. Juris, V. Balzani, P. Belser and A. von Zelewsky, *Helv. Chim. Acta*, 1981, **64**, 2175-2182.
22. K. Nakamaru, *J. Chem. Soc. Jpn.*, 1982, **55**, 2697-2705.
23. K. Dedeian, P. I. Djurovich, F. O. Garces, G. Carlson and R. J. Watts, *Inorg. Chem.*, 1991, **30**, 1685-1687.
24. K. A. King, P. J. Spellane and R. J. Watts, *J. Am. Chem. Soc.*, 1985, **107**, 1431-1432; L. Flamigni, A. Barbieri, C. Sabatini, B. Ventura and F. Barigelletti, *Top. Curr. Chem.*, 2007, **281**, 143-203.
25. A. B. Tamayo, B. D. Alleyne, P. I. Djurovich, S. Lamansky, I. Tsyba, N. N. Ho, R. Bau and M. E. Thompson, *J. Am. Chem. Soc.*, 2003, **125**, 7377-7387.
26. G. J. Barbante, E. H. Doeven, E. Kerr, T. U. Connell, P. S. Donnelly, J. M. White, T. Lópes, S. Laird, C. F. Hogan, D. J. D. Wilson, P. J. Barnard and P. S. Francis, *Chem. Eur. J.*, 2014, **20**, 3322-3332.
27. M. Mydlak, C. Bizzarri, D. Hartmann, W. Sarfert, G. Schmid and L. De Cola, *Adv. Funct. Mater.*, 2010, **20**, 1812-1820.
28. S. Zanarini, M. Felici, G. Valenti, M. Marcaccio, L. Prodi, S. Bonacchi, P. Contreras-Carballada, R. M. Williams, M. C. Feiters, R. J. M. Nolte, L. De Cola and F. Paolucci, *Chem. Eur. J.*, 2011, **17**, 4640-4647.
29. J. Truong, K. B. Spilstead, G. J. Barbante, E. H. Doeven, D. J. D. Wilson, N. W. Barnett, L. C. Henderson, J. M. Altimari, S. C. Hockey, M. Zhou and P. S. Francis, *Analyst*, 2014, **139**, 6028-6035.
30. S. Liu, P. Muller, M. K. Takase and T. M. Swager, *Inorg. Chem.*, 2011, **50**, 7598-7609; E. Kerr, E. H. Doeven, G. J. Barbante, T. U. Connell, P. S. Donnelly, D. J. D. Wilson, T. D. Ashton, F. M. Pfeffer and P. S. Francis, *Chem. - Eur. J.*, 2015, **21**, 14987-14995.
31. M. S. Lowry, J. I. Goldsmith, J. D. Slinker, R. Rohl, R. A. Pascal, Jr., G. G. Malliaras and S. Bernhard, *Chem. Mater.*, 2005, **17**, 5712-5719.
32. T. M. Monos, A. C. Sun, R. C. McAtee, J. J. Devery and C. R. J. Stephenson, *J. Org. Chem.*, 2016, **81**, 6988-6994.
33. L. Skorka, M. Filapek, L. Zur, J. G. Malecki, W. Pisarski, M. Olejnik, W. Danikiewicz and S. Krompiec, *J. Phys. Chem. C*, 2016, **120**, 7284-7294.
34. A. F. Henwood and E. Zysman-Colman, *Chem. Commun.*, 2017, **53**, 807-826.
35. C. K. Prier, D. A. Rankic and D. W. C. MacMillan, *Chem. Rev.*, 2013, **113**, 5322-5363; T. Koike and M. Akita, *Inorg. Chem. Front.*, 2014, **1**, 562-576.
36. A. Singh, K. Teegardin, M. Kelly, K. S. Prasad, S. Krishnan and J. D. Weaver, *J. Organomet. Chem.*, 2015, **776**, 51-59.
37. T. U. Connell, J. M. White, T. A. Smith and P. S. Donnelly, *Inorg. Chem.*, 2016, **55**, 2776-2790.
38. H. J. Bolink, E. Coronado, R. D. Costa, N. Lardies and E. Orti, *Inorg. Chem.*, 2008, **47**, 9149-9151; D. Tordera, M. Delgado, E. Orti, H. J. Bolink, J. Frey, M. K. Nazeeruddin and E. Baranoff, *Chem. Mater.*, 2012, **24**, 1896-1903.
39. R. D. Costa, E. Orti, H. J. Bolink, F. Monti, G. Accorsi and N. Armaroli, *Angew. Chem. Int. Ed.*, 2012, **51**, 8178-8211; S. Ladouceur, K. N. Swanick, S. Gallagher-Duval, Z. Ding and E.

Zysman-Colman, *Eur. J. Inorg. Chem.*, 2013, **2013**, 5329-5343.
40. M. S. Lowry and S. Bernhard, *Chem.-Eur. J.*, 2006, **12**, 7970-7977.
41. E. Orselli, R. Q. Albuquerque, P. M. Fransen, R. Fröhlich, H. M. Janssen and L. De Cola, *J. Mater. Chem.*, 2008, **18**, 4579-4590; M. Felici, P. Contreras-Carballada, Y. Vida, J. M. Smits, R. J. Nolte, L. De Cola, R. M. Williams and M. C. Feiters, *Chem. - Eur. J.*, 2009, **15**, 13124-13134; Z. M. Smith, E. Kerr, E. H. Doeven, T. U. Connell, N. W. Barnett, P. S. Donnelly, S. J. Haswell and P. S. Francis, *Analyst*, 2016, **141**, 2140-2144.
42. K. Hong, Y. K. Kwon, J. Ryu, J. Y. Lee, S. H. Kim and K. H. Lee, *Sci. Rep.*, 2016, **6**, 29805; H. C. Moon, T. P. Lodge and C. D. Frisbie, *J. Mater. Chem. C*, 2016, **6**, 8448-8453; S. H. Kong, J. I. Lee, S. Kim and M. S. Kang, *ACS Photonics*, 2018, **5**, 267-277.
43. S. Bonafede, M. Ciano, F. Bolletta, V. Balzani, L. Chassot and A. v. Zelewsky, *J. Phys. Chem.*, 1986, **90**, 3836-3841.
44. G. M. Sheldrick, *Acta Crystallogr., Sect. A: Found. Crystallogr.*, 2008, **64**, 112-122; G. M. Sheldrick, *Acta Crystallogr., Sect. C*, 2015, **71**, 3-8.
45. L. J. Farrugia, *J. Appl. Crystallogr.*, 1997, **30**, 565; L. J. Farrugia, *J. Appl. Crystallogr.*, 1999, **32**, 837-838.
46. P. S. Francis, J. L. Adcock and N. W. Barnett, *Spectrochim. Acta, Part A*, 2006, **65**, 708-710.
47. C. Mallet, A. Bolduc, S. Bishop, Y. Gautier and W. G. Skene, *Phys. Chem. Chem. Phys.*, 2014, **16**, 24382-24390.
48. M. J. Frisch, G. W. Trucks, H. B. Schlegel, G. E. Scuseria, M. A. Robb, J. R. Cheeseman, G. Scalmani, V. Barone, B. Mennucci, G. A. Petersson, H. Nakatsuji, M. Caricato, X. Li, H. P. Hratchian, A. F. Izmaylov, J. Bloino, G. Zheng, J. L. Sonnenberg, M. Hada, M. Ehara, K. Toyota, R. Fukuda, J. Hasegawa, M. Ishida, T. Nakajima, Y. Honda, O. Kitao, H. Nakai, T. Vreven, J. A. Montgomery, Jr., J. E. Peralta, F. Ogliaro, M. Bearpark, J. J. Heyd, E. Brothers, K. N. Kudin, V. N. Staroverov, R. Kobayashi, J. Normand, K. Raghavachari, A. Rendell, J. C. Burant, S. S. Iyengar, J. Tomasi, M. Cossi, N. Rega, J. M. Millam, M. Klene, J. E. Knox, J. B. Cross, V. Bakken, C. Adamo, J. Jaramillo, R. Gomperts, R. E. Stratmann, O. Yazyev, A. J. Austin, R. Cammi, C. Pomelli, J. W. Ochterski, R. L. Martin, K. Morokuma, V. G. Zakrzewski, G. A. Voth, P. Salvador, J. J. Dannenberg, S. Dapprich, A. D. Daniels, Ö. Farkas, J. B. Foresman, J. V. Ortiz, J. Cioslowski and D. J. Fox, Gaussian 09, Revision E.1, Gaussian, Inc., Wallingford CT, 2009.
49. A. D. Becke, *Phys. Rev. A: Gen. Phys.*, 1988, **38**, 3098-3100; J. P. Perdew, *Phys. Rev. B*, 1986, **33**, 8822-8824.
50. F. Weigend and R. Ahlrichs, *Phys. Chem. Chem. Phys.*, 2005, **7**, 3297-3305.
51. C. Adamo and V. Barone, *J. Chem. Phys.*, 1998, **108**, 664-675.
52. J. Tomasi, B. Mennucci and R. Cammi, *Chem. Rev.*, 2005, **105**, 2999-3093.
53. A. V. Marenich, C. J. Cramer and D. G. Truhlar, *J. Phys. Chem. B*, 2009, **113**, 6378-6396.
54. A. L. Tenderholt, QMForge, Version 2.4, http://qmforge.sourceforge.net

Table of Contents Image

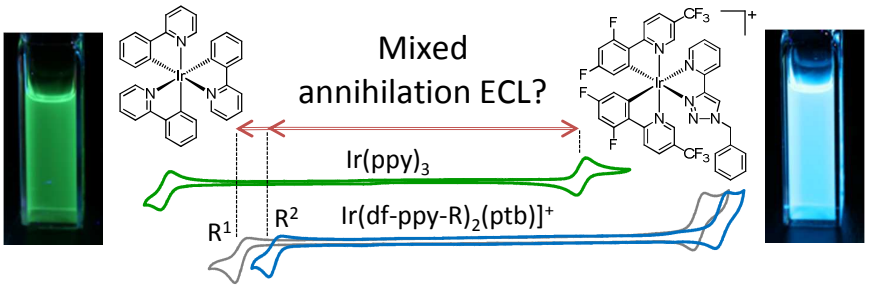

The annihilation electrogenerated chemiluminescence of mixtures of Ir(III) complexes is eliminated by manipulating reduction potentials through subtle changes in ligand structure.